

IONIC LIQUID–ELECTRODE INTERFACE: CLASSIFICATION OF IONS, SATURATION OF LAYERS, AND STRUCTURE-DETERMINED POTENTIALS

Karl Karu ¹, Eva Roos Nerut ¹, Xueran Tao ¹, Sergei A. Kislenko ^{2,3}, Kaija Pohako-Esko ⁴, Iuliia V. Voroshyllova ^{5*}, Vladislav B. Ivanišťev ^{6*}

¹ Institute of Chemistry, University of Tartu, Ravila 14a, 50411 Tartu, Estonia

² Joint Institute for High Temperatures, Russian Academy of Sciences, Moscow, 125412 Russia

³ Moscow Institute of Physics and Technology (State University), Dolgoprudnyi, Moscow oblast, 141700 Russia

⁴ IMS Lab, Institute of Technology, University of Tartu, Nooruse 1, 50411 Tartu, Estonia

⁵ LAQV@REQUIMTE, Faculdade de Ciências, Universidade do Porto, Departamento de Química e Bioquímica, Rua do Campo Alegre, 4169-007 Porto, Portugal

⁶ Department of Chemistry, Center for High Entropy Alloy Catalysis, University of Copenhagen (UCPH), 2100 Copenhagen Ø, Denmark

* Correspondence: vladislav.ivaništsev@ut.ee, voroshyllova.iuliia@fc.up.pt

Abstract

With a single-electrode model, we investigated surface charge screening at an ionic liquid–electrode interface. Using the obtained geometric packing densities, we estimated structure-determined potentials and capacitance values for 40 studied ions. By comparing the predictions with the empirical data, we show that exact surface charge screening by a monolayer of counter-ions (as well as crowding of ions) is improbable for common ions within their electrochemical stability window. We also predict that theoretically such a screening state is possible for frisbee-shape ions.

Keywords: potential of monolayer charge, maximum packing density, ionic liquids, molecular dynamics simulations, electrical double layer, overscreening, crowding, interface.

1.1. Introduction

The potential of applying ionic liquids (ILs) in technological applications motivates extensive studies of the electrical double layer (EDL) at IL-electrode interfaces. Remarkable advances have been reached in the experimental characterisation of such interfaces. Namely, the unique layering of ions near the electrode surface (known as *overscreening*) was accessed with an impressively wide range of spectroscopy [1–15], microscopy [16–28], and electrochemistry techniques [29–43]. Moreover, the theoretically predicted *crowding* of counter-ions [44–47] was observed in computer simulations [48–52]. According to simulations, the overscreening-to-crowding transition corresponds to the maximum density of ions packed in a monolayer of counter-ions [53–55], which appears in various molecular dynamics (MD), Monte Carlo, and classical density functional theory studies [50,51,56]. However, neither crowding nor monolayer formation have been decisively demonstrated in experiments [12,13,15,40,41,57].

Previously, the maximum packing density of IL ions (θ_M) was evaluated for a limited set of ions in work [58] with a conclusion that the monolayer of practically important ions (like Im_4^+ , TFSI^- , FEP^-) is unlikely to form under experimental conditions. In this work, with the help of MD simulations, we calculated θ_M for a larger set of ions with different sizes and shapes (see [Figure 1](#)). Below we describe how θ_M and related structure-determined values can guide the experimental characterization of crowded EDL and tuning (electro/mechano)chemical properties of IL-electrode interfaces in practical applications.

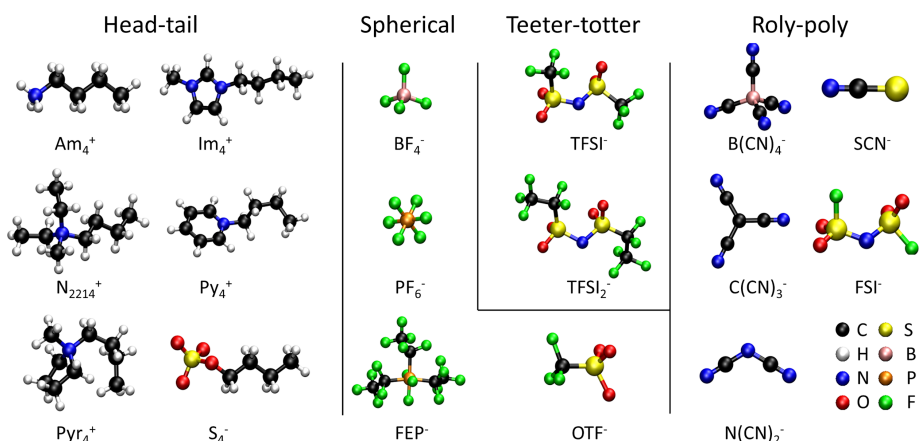


Figure 1: Ball-and-stick model of selected ions representing four identified classes. For ion names and acronyms see the Appendix Table 1.

1.2. Methods

1.2.1. Phenomenological model

In this work, we use the ionic bilayer model which simplifies the layered IL-electrode interface to two layers, so that the contact layer of counter-ions overscreens the surface charge and the subsequent layer neutralizes the charge excess. The ionic bilayer model is described in detail in our previous works [REF]. In this work, let us focus on structure-determined potentials (φ_S and φ_M) and capacitances (C_S and C_M):

$$C_S = C_H \text{ and } C_M = aC_H \quad (1)$$

and

$$\varphi_S = \frac{\theta_M}{C_H} \left(\frac{1}{a} \right)^{\frac{1}{a-1}} \text{ and } \varphi_M = \frac{\theta_M}{C_H} \quad (2)$$

where a is the scaling exponent, C_H is the Helmholtz capacitance, θ_M is the maximum packing density. The SI includes derivation of Eqs. 1 and 2 along with a detailed description of all quantities. Below we present the evaluated θ_M and estimated (C_M , φ_M) and (C_S , φ_S) values for 40 ions.

1.2.2. Computer model

The EDL in ILs is commonly simulated using two-electrode models with IL electrolyte between them [59,60]. The two-electrode model allows applying constant surface charge, constant potential, and constant field method in the simulations [61–63]. Bisection of a two-electrode model gives a single-electrode EDL model that is commonly applied in electrocatalysis simulations [64]. In the one-electrode model, counter- and co-ions compensate for the surface charge as schematically shown in [Figure 2](#).

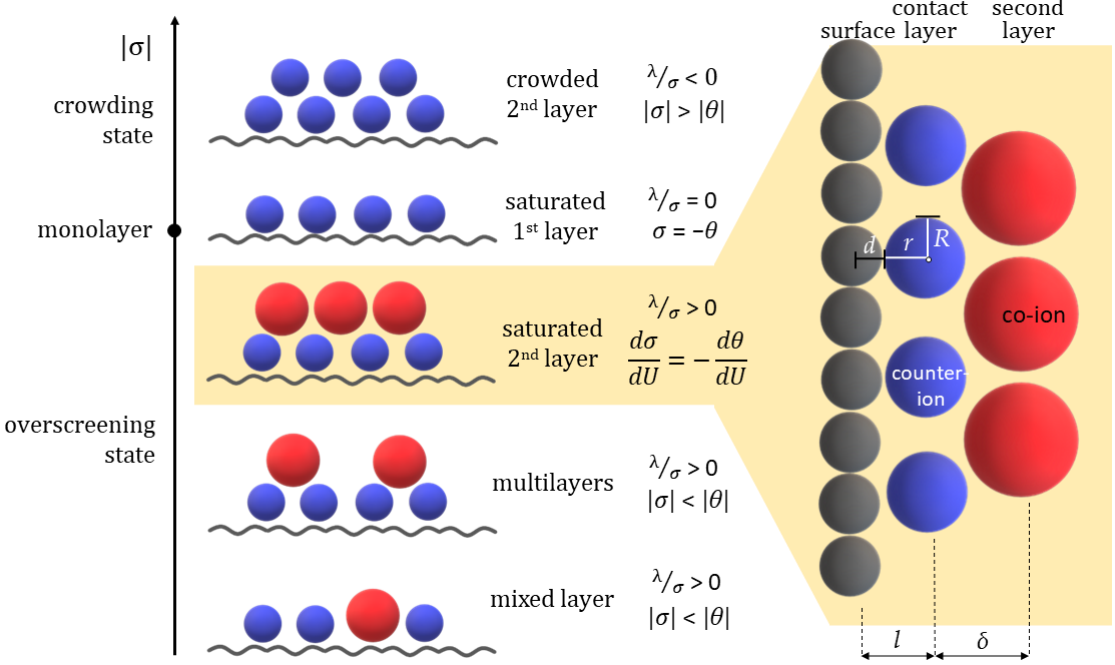


Figure 2: Schematic representation of an ionic liquid-electrode interface at variable surface charge density that is screened by shown counter- and co-ions. The given criteria are discussed in the text.

In this work, we used a single-electrode EDL model that includes only counter-ions as in the Helmholtz model. The graphene-like electrode was prepared using the Atomic Simulation Environment [65] with size $4.26 \text{ nm} \times 3.94 \text{ nm}$ (640 carbon atoms) and a 0.30 nm tolerance for packing. The Packmol software [66] was used to generate five replicas with different packing for a variable number of counter-ions.

We used that model in order to evaluate the maximum packing density (θ_M) under the assumption that this quantity is determined by the geometry of ions. From previous simulations, it is known that when $\sigma = -\theta_M$, the monolayer of counter-ions completely screens the surface charge density [54]. On that basis, we assume that the θ_M and φ_M values are similar for the simulations of our model and the more sophisticated two-electrode models. Herewith, the described simplification shortens the simulation time by two orders of magnitude in comparison to the two electrode models.

1.2.3. Molecular dynamics simulations

The simulations were performed with the GROMACS software [67–73] and OPLS-AA force fields with $\pm 1e$ ionic charges. First, a rough energy minimization run was

performed with a steep integrator for 10 ps with 1 fs timestep. Then, an equilibration step was run for 20 ps with 0.5 fs timestep, generating velocities corresponding to the temperature of 100 K. The production run was done in the Canonical ensemble (*NVT*) for 1000 ps with 1 fs time step and velocities corresponding to 353 K. The Verlet cut-off scheme was employed and *xy*-periodic boundary conditions were applied with the particle-mesh Ewald and 3dc Ewald correction [74–76]. Next, the trajectories excluding the first 10 ps of the production run were analyzed. Charge and mass density profiles as well as electrostatic potential profiles were obtained using GROMACS tools and processed using python scripts. MDanalysis software was used to analyze the distances [77,78]. Visualization was run with the VMD software [79].

1.2.4. Density functional theory calculations

Density functional theory calculations were performed to estimate the reduction and oxidation potentials of the IL ions. The calculations were performed using the r²SCAN-3c method [80] as implemented in the Orca 5.0.2 quantum chemistry program package [81]. The r²SCAN-3c is a composite method based on a meta-generalized-gradient approximation density functional [82,83], which employs a custom triple-zeta Gaussian basis set [80], D4 dispersion correction [84,85], and geometrical counterpoise correction [86]. The SCAN functional demonstrated great accuracy for determining the energetic parameters of IL ions, especially when paired with dispersion and counterpoise corrections. [87]

The geometries of the ions were optimized using nominal charges of +1e for cations and -1e for anions. Furthermore, single-point calculations were performed to calculate the ionization potential and electron affinity using these geometries with ionic charge of 0e and +2e for cations, and -2e and 0e for anions. Under the assumptions, that oxidation and reduction occur adiabatically and are not affected by the environment, for each anion–cation combination we estimated the IL electrochemical window as

$$EW = \min(IP) - \max(EA) \quad (10)$$

1.2.5. Structure-determined packing density, potential drops, and capacitances

The contact layer density (θ) was extracted from number density profiles, using the numerical evaluation of the density slices. Moving from the electrode to the opposing end of the simulation box, the beginning of the contact layer was defined as the point where the density in a slice exceeds an arbitrary threshold and the end of the contact layer as the point where the density drops back below the threshold. The density of a contact layer is found by integrating the density for the slices in between. [Figure 3](#) illustrates that the maximum packing density (θ_M) value corresponds to plateau at $|\theta|$ vs. $|\sigma|$ plot. The results were visually checked with VMD software for the crowding condition.

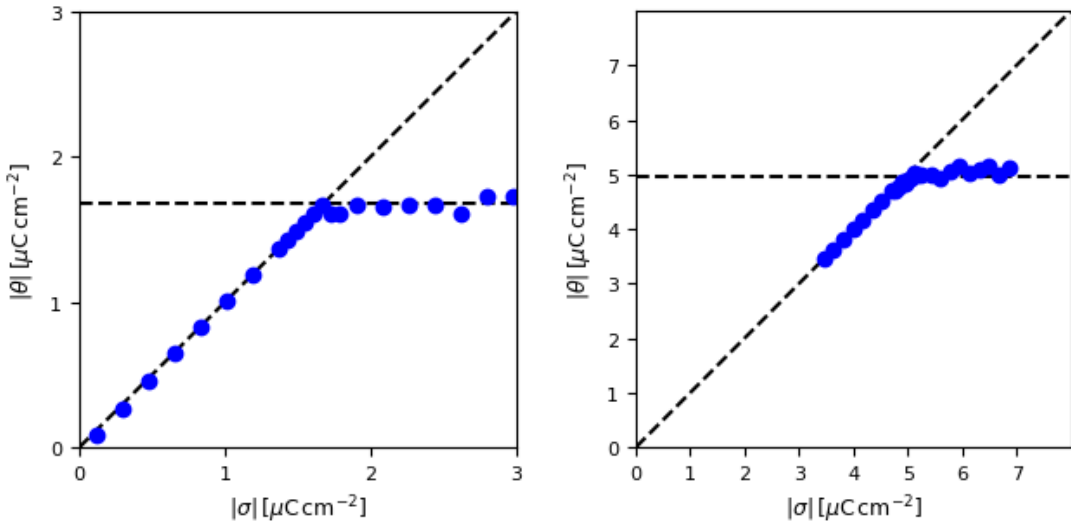


Figure 3: Contact layer charge density (θ) dependence on the surface charge density (σ) for PF_6^- . The maximum packing density (θ_M) corresponds to the plateau. Number of FEP^- and PF_6^- ions in the contact layer depends on the total number of counter-ions in simulations with (a) one and (b) two electrodes. The maximum packing density corresponds to the plateau.

The monolayer potential drop (φ_M) was calculated using the Poisson equation and the charge density profiles at estimated θ_M . Then we recalculated the φ_M values under two assumptions: first, the partial charge transfer can be accounted for by varying relative permittivity (ϵ_r); second, the total potential drop can be split into electrode and electrolyte contributions.

The first assumption views the partial charge transfer as an extreme on electronic polarization in the EDL. In our simulations, we used $\epsilon_r = 1$, while values from 1.6 to 2 are commonly used in MD simulations to account for electronic polarization through atomic charge scaling as $q = \epsilon_r^{-1/2}$ [67].

The second assumption was tested by comparing φ_M values evaluated directly *via* the Poisson equation ($\varphi_{M,p}$) and using simulated θ_M in the following expression with $q = \pm 1$ and $\epsilon_r = 1$:

$$\varphi_{M,G} = -\frac{d+r}{\epsilon_r \epsilon_0} \theta_M = -\frac{d\theta_M}{\epsilon_r \epsilon_0} + \frac{r}{R} \cdot \frac{q}{\epsilon_r \epsilon_0} \sqrt{\frac{\theta_M}{4q}} \quad (11)$$

where d is the surface atom's radius, q is the counter-ion charge ($\pm 1e$ in this study), r/R is the compression factor of an ion, *i.e.* the ratio between contact (r) and lateral (R) radii of the counter-ion. The lateral radius was calculated as $R^2 = 1/4 \cdot q/\theta_M$. The compression factor indicates how much the ion's elliptic form deviates from a spherical form. The summation of d and r assumes that the distance between the surface and the contact layer is given by the radii of surface atoms and counter-ions. That assumption is supported by the high coefficients of determination (R^2) of 0.988 for linear regression of $\varphi_{M,p}$ and $\varphi_{M,G}$ values (see the SI). Indeed, the potential drop within distance d from the electrode can be associated with the electrode and corrected as described in Ref. [68]. So, we set $d = 0$ nm in Eq. (11) by assuming that the surface charge plane of an ideal metal electrode extends by one-half of an interplanar spacing as follows from theory [69,70] and calculations [71,72]. Below we report $\varphi_M - C_M$ and $\varphi_s - C_s$ pair values calculated from θ_M and r values using Eqs. (5)–(11) with $l = r$ ($d = 0$) and $\epsilon_r = 2$.

1.3. Results

1.3.1. Taxonomy of counter-ions

The examined ions were categorized into four distinct classes according to their packing features: ball, head-tail, roly-poly, and teeter-totter. The interfacial behavior was differentiated by the $-\theta(\sigma)$ dependence like in [Figure 3](#). The ball and teeter-totter ions give a simple $|\theta| - \sigma$ plot with two clear intersecting lines, while head-tail and roly-poly ions give more complex $|\theta| - \sigma$ plots due to the reorientation of individual ions.

1.3.2. Ball class

The ball class, as its name suggests, includes roundish ions such as BF_4^- , Br^- , Cl^- , FEP^- , I^- , OTF and PF_6^- . Their main packing feature is that they behave like coarse-grained spheres during the simulations and form close-packed structures.

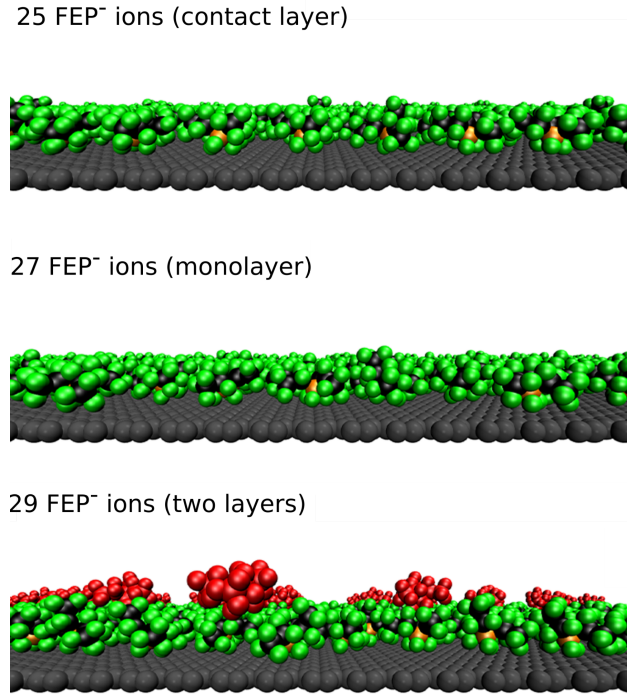


Figure 4: Side view on the ball-and-stick models of the FEP^- | electrode interface. The maximum packing density is reached in simulations of 27 FEP^- ball ions per electrode area. Ions forming the second layer are shown in red.

[Figure 4](#) shows the packing of ball FEP^- ions. Due to the simple shape, ions are well organized and fill the surface in a highly ordered manner resulting in dense packing. Ions belonging to this class do not change orientations upon increasing $|\sigma|$. However, their packing density can increase stepwise with increasing $|\sigma|$. In [Figure 5](#), the packing density is increasing stepwise from -150 to $-162 \mu\text{C}\cdot\text{cm}^{-2}$ when σ is increased by only 1 $\mu\text{C}\cdot\text{cm}^{-2}$ (one ion per model). A similar phenomenon is well known for halide anions that adsorb specifically from aqueous solutions [74]. Analogues stepwise densening was also observed in MD simulations of $\text{Au}(hkl) | \text{BMImPF}_6$ interfaces [88].

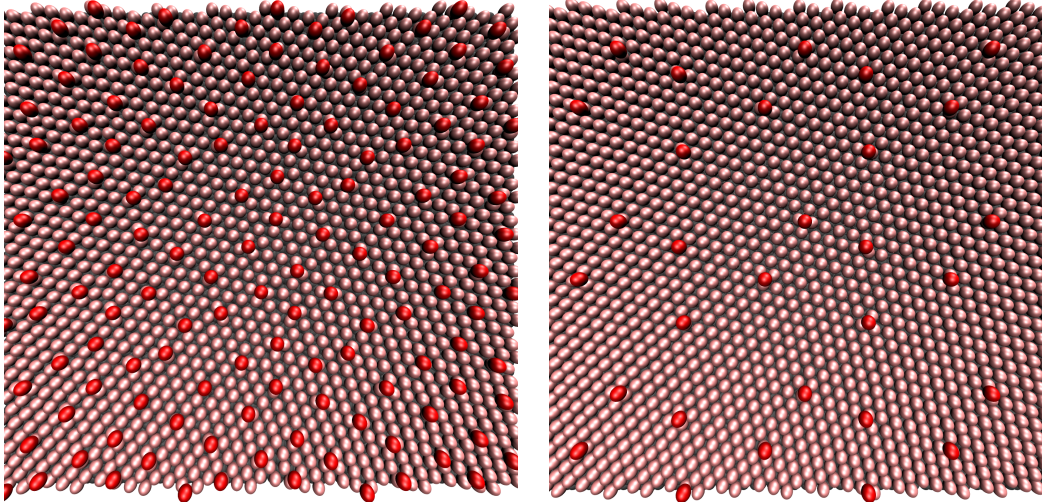


Figure 5: Top view on Br^- adlayers. Ions in the first layer are shown in pink (lighter) and in the second layer are shown in red (darker). The surface atoms are not seen. Left: model with 173 ions, 157 of which are in the contact layer. Right: model with 174 ions, 170 of which are in the contact layer.

[Table 1](#) summarizes simulated and estimated parameters of the modeled IL–electrode interfaces with ball ions. This data is discussed below.

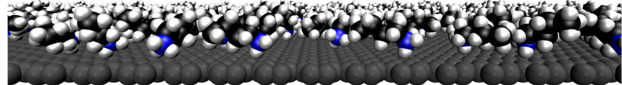
Table 1: Structure-determined parameters of the modeled EDLs with ball ions.

Ion	θ_M [$\mu\text{C}\cdot\text{cm}^{-2}$]	φ_M [V]	φ_S [V]	C_M [$\mu\text{F}\cdot\text{cm}^{-2}$]	C_s [$\mu\text{F}\cdot\text{cm}^{-2}$]	r [nm]	R [nm]	a
BF_4^-	-105.95	10.5	1.9	3.1	10.1	3.1	5.15	0.60
Br^-	-149.85	9.5	1.5	4.0	15.7	2.6	6.12	0.26
Cl^-	-182.30	9.7	1.5	4.4	18.9	2.5	6.75	0.23
FEP^-	-25.77	3.8	0.8	2.5	6.7	3.8	2.54	0.37
I^-	-86.86	7.4	1.2	3.0	11.8	2.9	4.66	0.26
OTF^-	-73.49	7.8	1.2	2.2	9.4	3.2	4.29	0.39
PF_6^-	-78.27	10.8	2.2	2.6	7.3	3.7	4.42	0.60

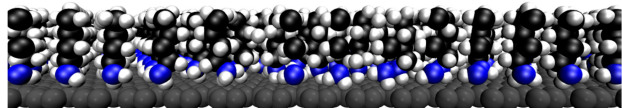
1.3.3. Head-tail class

Head-tail ions consist of an alkyl chain tail and a head, holding the ionic charge. For Py_n^+ and Im_n^+ the head is an aromatic cycle. For Am_n^+ , Pyr_n^- and N_{2214}^+ ions, the head is an (alkyl)ammonium group.

29 AM_4^+ ions (contact layer)



103 AM_4^+ ions (monolayer)



104 AM_4^+ ions (two layers)

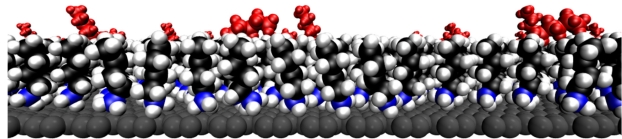


Figure 6: Side view on the ball-and-stick models of the Am_4^+ | electrode interface. The maximum packing density is reached in simulations of 103 Am_4^+ ions per electrode area. Ions of the second layer are shown in red.

[Figure 7](#) shows layers of head-tail Am_4^+ ions. While at low $|\sigma|$ there are enough voids on the surface, Am_4^+ tails lie down parallel to the surface. At high $|\sigma|$, Am_4^+ tails are forced to “stand up”, *i. e.* point outwards the surface to free void and facilitate surface charge screening by Am_4^+ heads. Similar phenomenon was described in detail from MD simulations of EDLs with N_{1114}^+ , N_{1144}^+ , N_{1444}^+ , and N_{4444}^+ ions [13]. In the monolayer, all Am_4^+ tails are oriented outwards from the surface. Similar pictures are seen for all studied head-tail ions: first, in the overscreening state their tails can reorient; second, prior and in the crowding state the EDL structure depends on the head-tail form and size. Let us describe five scenarios:

(1) **Head reorientation:** In the case of Im^+ and Py^+ ions, their aromatic rings (heads) change orientation from parallel to perpendicular relative to the surface. For example, in the Im^+ monolayer, there are three distinguishable orientations of the Im^+ ring: parallel and perpendicular to the surface with C^2 pointing towards and outwards the surface. Such orientation resembles lying, standing downwards, and standing upwards at the surface and were observed in numerous MD simulations and experimental works. [76,89–91]

(2) **Head-head stacking:** Ions that do not fit their head into the contact layer occupy voids between tails right above the contact layer heads, thus, appearing as head-to-head stacking.

(3) **Head-tail intercalation:** Ions that do not fit their head into the contact layer occupy voids between tails at a distance from the contact layer heads, thus, appearing as intercalating the layer of tails.

(4) **Heads over tails crowding:** Ions that do not fit their head into the contact layer situated above the layer of tails. In Figure 7, such ions can not penetrate the layer of tails due to a very dense packing of Am_n^+ in the contact layer. The longer the tail the denser the layer of tails. Thus, even if head-head stacking and head-tail intercalation is possible for ions with short tails and large heads, when the tails become longer, a larger fraction of ions crowd above the tails.

(5) **Tail-tails stacking:** Such behavior, described in “Monolayer to Bilayer Structural Transition in Confined Pyrrolidinium-Based Ionic Liquids” by Smith *et al.*, has not been observed in our simulations [92–94]. Differently from the experiments, where such transition was induced by increasing n from 8 to 10, our simulations might not reproduce that bilayer structure due to the absence of co-ions that stabilizes the transition.

[Table 2](#) summarizes simulated and estimated parameters of the modeled EDLs with head-tail ions with the tail length of 4. Additional data is given in the [SI Table 2](#).

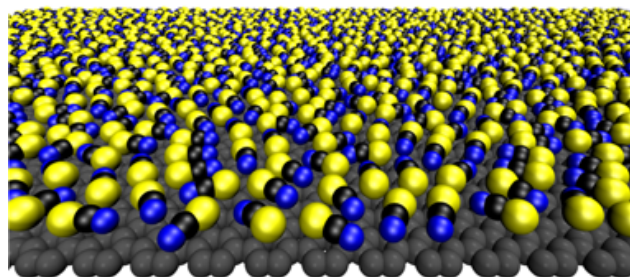
Table 2: Structure-determined parameters of the modeled EDLs with head-tail ions. Only one set is shown per each family of ions, while more detailed data can be found in the [SI Table 2](#).

Ion	θ_M [$\mu\text{C}\cdot\text{cm}^{-2}$]	φ_M [V]	φ_S [V]	C_M [$\mu\text{F}\cdot\text{cm}^{-2}$]	C_S [$\mu\text{F}\cdot\text{cm}^{-2}$]	r [nm]	R [nm]	a
AM_4^+	98.31	-4.4	-1.2	13.5	22.5	2.3	4.96	0.60
IM_4^+	44.86	-4.1	-1.0	5.4	10.9	3.0	3.35	0.50
Py_4^+	42.95	-3.8	-1.1	7.9	11.3	3.0	3.28	0.69
Pyr_4^+	46.77	-6.9	-2.1	4.8	6.7	3.8	3.42	0.71
N_{2214}^+	43.91	-7.4	-1.6	2.2	5.9	4.1	3.31	0.95
S_4^-	65.86	1.5	21.8	3.5	9.1	3.3	4.06	0.39

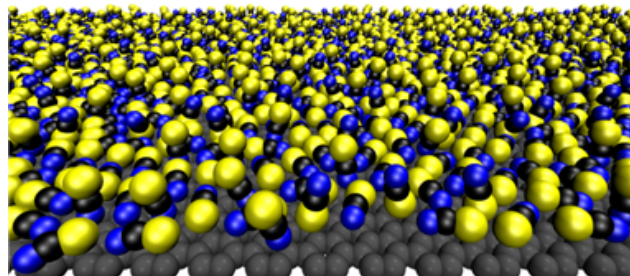
1.3.4. Roly-poly class

Roly-poly ions, as the class name suggests, can change individual orientation from parallel to perpendicular to the surface with increasing $|\sigma|$. Roly-poly ions prefer to lie flat on the surface at low $|\sigma|$, but as $|\sigma|$ increases to a certain point, ions begin to stand up to make more void for adsorbing ions. [Figure 7](#) shows a particular state where all ions lie parallel to the surface. Increasing $|\sigma|$ forces ions to stand up increasing the fraction of ions oriented perpendicular to the surface. In the monolayer of roly-poly ions, we observed that both parallel and perpendicular orientations coexist. Moreover, roly-poly ions can stand both up and down. In [Figure 7](#), the SCN^- ions contact the surface with both sulfur and nitrogen atoms. In general, roly-poly ions are drastically different from head-tail and ball ions in terms of packing at variable $|\sigma|$.

83 SCN⁻ ions (contact layer)



110 SCN⁻ ions (monolayer)



128 SCN⁻ ions (two layers)

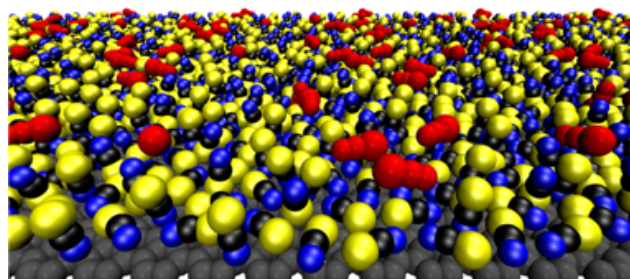


Figure 7: Side view on the ball-and-stick models of the SCN⁻ | electrode interface. First SCN⁻ stands when 86 ions are simulated, and the maximum packing density is reached when 110 SCN⁻ ions are simulated per electrode area. Ions of the second layer are shown in red.

[Table 3](#) summarizes simulated and estimated parameters of the modeled EDLs with roly-poly ions. This data is discussed below.

Table 3: Structure-determined parameters of the modeled EDLs with roly-poly and teeter-totter (TFSI_n^-) ions.

Ion	θ_M [$\mu\text{C}\cdot\text{cm}^{-2}$]	φ_M [V]	φ_s [V]	C_M [$\mu\text{F}\cdot\text{cm}^{-2}$]	C_s [$\mu\text{F}\cdot\text{cm}^{-2}$]	r [nm]	R [nm]	a
$\text{B}(\text{CN})_4^-$	-66.81	11.8	3.1	3.0	5.7	4.2	4.09	0.96
FSI^-	-58.22	7.0	1.3	2.7	8.3	3.4	3.82	0.33
$\text{C}(\text{CN})_3^-$	-73.49	8.3	2.0	4.3	8.9	3.3	4.29	0.48
$\text{N}(\text{CN})_2^-$	-110.72	9.4	1.5	3.0	11.8	2.9	5.26	0.26
SCN^-	-104.99	5.2	0.6	3.6	20.2	2.4	5.12	0.18
TFSI^-	-42.00	4.6	1.1	4.6	9.1	3.3	3.24	0.50
TFSI_2^-	-31.50	3.6	0.8	3.9	8.9	3.3	2.81	0.44

1.3.5. Teeter-totter class

Teeter-totter ions are composed of ions which have a binary structure with one central atom connecting two similar groups on both sides.

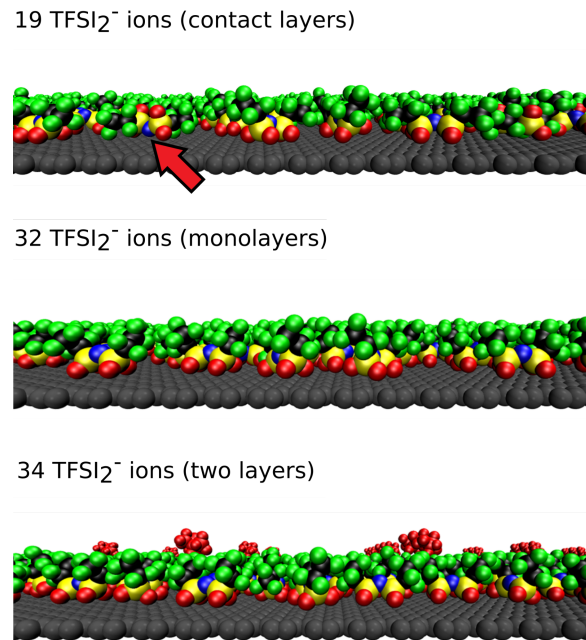


Figure 8: Side view on the ball-and-stick models of the $\text{TFSI}_2^- \mid$ electrode interface. The maximum packing density is reached when 31 TFSI_2^- ions are simulated per the electrode area. Ions of the second layer are shown in red. One trans-configuration ion is indicated with a red arrow.

Even though the teeter-totter ions can be considered having a linear shape and similar to the roly-poly ions, they do not reorient with increasing $|\sigma|$. Only at very low $|\sigma|$, the teeter-totter ions might take a trans-configuration as marked in [Figure 8](#), and in agreement with experimental results [12]. More negatively charged atoms of teeter-totter ions face down the surface at all studied $|\sigma|$.

1.3.6. Summary of results

All evaluated $\varphi_{M,P} - \theta_M$ values along with the curve following Eq. [\(11\)](#) are shown in [Figure 9](#). Judging by the compression factor (r/R), it is apparent that most of the ions are ellipses (like TFSI_n^- and heads of Am_n^+ and S_n^- with $r/R \approx 0.4$), some ions are slightly more roundish (halide anions and Py_n^+ with $r/R \approx 0.6$), while others are almost round (cyano-based anions and Pyr_n^+ with $r/R \approx 0.8$). For ball ions, [Figure 9](#) shows an obvious trend of rising φ_M value with decreasing ion radius. As a clear example, for halide ions, the smaller the ion, the higher the potential of the monolayer formation. This observation goes *qualitatively* inline with predictions made by Ivaniščev and Fedorov [95], where the maximum packing density was approximated $\theta_M = \frac{1}{4} \cdot q/R^2$.

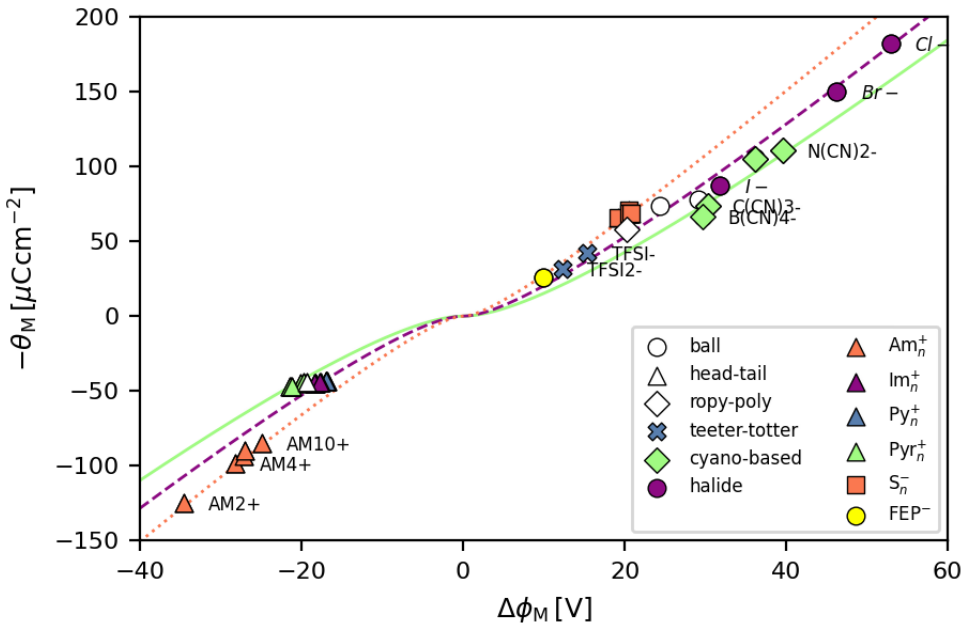


Figure 9: Calculated maximum packing density (θ_M) and monolayer potential drop ($\varphi_{M,P}$) values. Lines follow Eq. [\(13\)](#) with compression factor (r/R) of 0.8 (solid), 0.6 (dashed), and 0.4 (dotted).

For head-tail ions, using radii from Refs. [77,78,96], Ivaništšev and Fedorov predicted a dependence of θ_M on the tail length [95]. However, in the presented simulations, only θ_M of Am_n^+ depends on the tail length. Differently from all simulated head-tail ions, in Am_n^+ the ammonium head and alkyl tail have a similar cross-section diameter, so that the stacking of tails determines the packing of heads as can be seen in [Figure 6](#). The lateral distance between tails increases with the number of bent conformations, *i. e.* the tail lengthening. That effect is leveled when the head is wider than the tail, like in Im_n^+ , Py_n^+ , and Pyr_n^+ yielding almost the same θ_M value for these ions (see [Figure 9](#)).

2. Discussions

2.1. Comparison of structure-determined potentials

[Figure 10](#) summarizes all corrected $\varphi_M - \theta_M$ values from Tables 1–3 and [SI Table 2](#). The correction of the values obtained with the Poisson equation includes: (1) shifting the surface charge plane by $-d\theta_M/\epsilon_0$ with $d = 0.17$ nm and (2) dividing by $\epsilon_r = 2$. The shown θ_M values correspond to the ion charge $q = \pm 1e$ as in [Figure 9](#) and all Tables.

The most marked feature is that all φ_M values are outside the ± 2 V vs PZC region, which is the experimentally measurable potential window [58]. In other words, for all studied ions, the true monolayer formation and crowding should not be experimentally reachable. That conclusion holds under the assumption that the partial charge transfer is below $1 - \sqrt{\frac{1}{2}} = 0.3e$. The highly polarizable Py_n^+ could form the monolayer at -2 V upon accepting $0.5e$ (see [Figure 10](#)) and halide anions could form their monolayers at $+2$ V upon donating $0.7e$. The scanning tunneling microscopy study of Py_4^+ adsorption from Py_4BF_4 did not reveal any ordered structure [97]. On the opposite, halide anions are well known for forming highly ordered adlayers even at lower relative potentials [82,98]. Thus, it is worth examining whether these adlayers meet the monolayer definition by checking for evidence of overscreening and crowding. For instance, by examining composition of the second layer with XRD and STM [99].

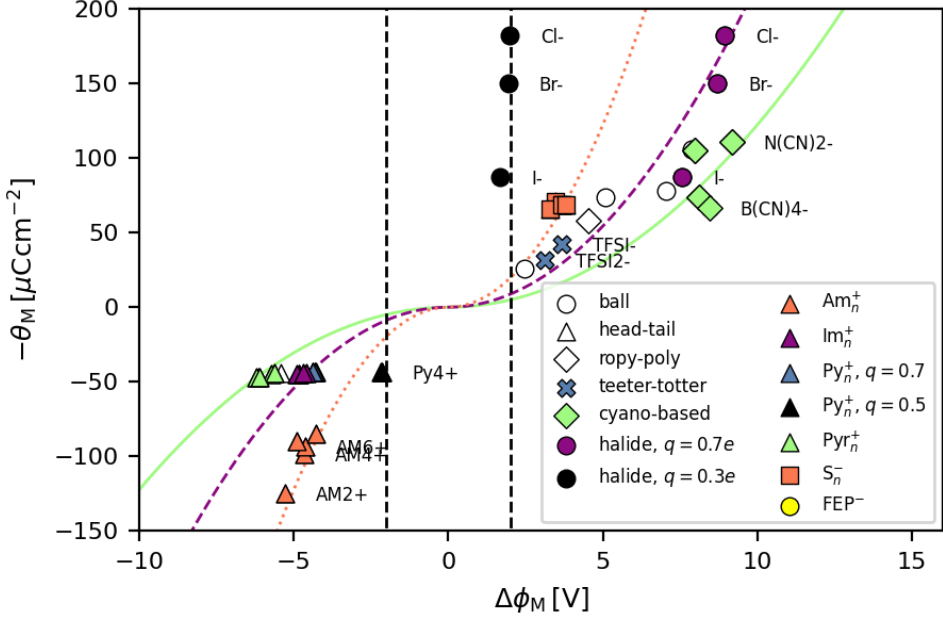


Figure 10: Simulated maximum packing density (θ_M) and recalculated monolayer potential drop (ϕ_M) values. Lines follow Eq. (13) with $d = 0$, $\epsilon_r = 2$, and compression factor (r/R) equals 0.8 (solid), 0.6 (dashed), and 0.4 (dotted).

A notable finding of this work is that estimated φ_S values are within the ± 2 V region as can be seen in Tables 1–4. We suggest that most of the reported ordered adlayers [16,18,22,37,39,83–85,87,100] form in the vicinity of the saturation potential (φ_S). Let us illustrate this conclusion with Figure 2 showing the results of two electrode simulations of BMImPF₆ [55], where φ_S of 3 V was estimated for PF₆⁻ anions. In this work, the corresponding estimation is 2.2 V with $\epsilon_r = 1.6$ as in the referred MD simulations. Despite crude approximations in Eq. (11) for φ_S , it leads to a phenomenologically reasonable conclusion that previously reported interfacial processes [100,101] are most probably happening in the overscreening state which is far from crowding.

2.2. Ion shape and the monolayer potential

Let us use the obtained data to answer an essential question – whether monolayers of physisorbed ions are in principle achievable. The criteria for such a possibility is a realistically low $|\varphi_M|$ value below 2 V. For the ball ions, the potential can be translated into a radius of over 1.13 nm assuming that $\epsilon_r = 2$ and $d = 0$ in Eq. (13). In other words, hard ball ions of $\pm 1e$ charge and 1.13 nm radius form a monolayer at ∓ 2 V. All studied

and most known ILs ions have much smaller dimensions. Let us take for example a polyoxometalate $\text{PW}_{12}\text{O}_{40}^{3-}$ anions that was discussed by Borukhov *et al.* in Refs. [102,103] to illustrate the idea of crowding. $\text{PW}_{12}\text{O}_{40}^{3-}$ has a radius of 0.55 nm and an ion charge of $-3e$. A simple estimation of φ_M for $\text{PW}_{12}\text{O}_{40}^{3-}$ gives an unreachable potential value of +13 V!

[Figure 10](#) hints at the way of lowering the φ_M by decreasing the compression factor. Indeed a flat and wide frisbee-shaped cation with $r = 0.17$ nm and $R = 0.44$ nm should form a monolayer at -2 V. That is comparable to the size of $3N$ -coronene cations – one of the smallest representatives of nitrogen-substituted polycyclic aromatic hydrocarbon (PAH) cations [104]. Similar PAH could be substituted with boron [105] to give frisbee anions. To the best of our knowledge, such PAH-based ILs are unknown. Yet, numerous experiments with triangulenium cations visualized ordered adlayers [106,106,107]. More realistic estimations (with $d > 0$ and $\varepsilon < 2$) imply that larger PAH ions are potential candidates for crowding at relatively small potentials. Experimental and computational study of such ions promises the discovery of exciting new phenomena.

2.3. Concluding remarks and future research directions

By comparing the estimated φ_M and φ_s values to empirical data, we conclude that the monolayer and crowded structures of studied ions are unreachable within experimentally measurable potential windows. Our data along with the classification of ions suggest designing frisbee-shaped ions that can form crowded structures. Reaching the crowded state can reveal new phenomena of high application potential as predicted and discussed in Ref. [108]. For the common ions, we conclude that previously observed adlayers of such ions are formed in the vicinity of φ_s , *i. e.*, in the overscreening state. It is also essential to understand the nature of these adlayers at surface from both fundamental and application perspectives.

2.5. Acknowledgements

This work was supported by the Estonian Research Council Institutional Research Grant IUT20–13, and Estonian Personal Research Project PUT1107. Part of the work was performed under research contract no. 796/RPSA with the Skolkovo Institute of Science

and Technology. The EU supported this research through the European Regional Development Fund (TK141 “Advanced materials and high-technology devices for energy recuperation systems”). The financial support from FCT/MCTES through the Portuguese national funds, project No. UID/QUI/50006/2021 (LAQV@REQUIMTE) is also acknowledged. Results were obtained in part using the High Performance Computing Center of the University of Tartu.

2.6. References

- [1] G. Velpula, R. Phillipson, J.X. Lian, D. Cornil, P. Walke, K. Verguts, S. Brems, H. Uji-i, S. De Gendt, D. Beljonne, R. Lazzaroni, K.S. Mali, S. De Feyter, Graphene Meets Ionic Liquids: Fermi Level Engineering via Electrostatic Forces, *ACS Nano*. 13 (2019) 3512–3521. <https://doi.org/10.1021/acsnano.8b09768>.
- [2] S. Xu, S. Xing, S.-S. Pei, V. Ivaništšev, R. Lynden-Bell, S. Baldelli, Molecular Response of 1-Butyl-3-Methylimidazolium Dicyanamide Ionic Liquid at the Graphene Electrode Interface Investigated by Sum Frequency Generation Spectroscopy and Molecular Dynamics Simulations, *J. Phys. Chem. C*. 119 (2015) 26009–26019. <https://doi.org/10.1021/acs.jpcc.5b08736>.
- [3] A.B. Biedron, E.L. Garfunkel, E.W. Castner, S. Rangan, Ionic liquid ultrathin films at the surface of Cu(100) and Au(111), *J. Chem. Phys.* 146 (2017) 054704. <https://doi.org/10.1063/1.4975101>.
- [4] M. Chu, M. Miller, T. Douglas, P. Dutta, Ultraslow Dynamics at a Charged Silicon–Ionic Liquid Interface Revealed by X-ray Reflectivity, *J. Phys. Chem. C*. 121 (2017) 3841–3845. <https://doi.org/10.1021/acs.jpcc.6b10443>.
- [5] R. Yamamoto, H. Morisaki, O. Sakata, H. Shimotani, H. Yuan, Y. Iwasa, T. Kimura, Y. Wakabayashi, External electric field dependence of the structure of the electric double layer at an ionic liquid/Au interface, *Appl. Phys. Lett.* 101 (2012) 053122. <https://doi.org/10.1063/1.4742920>.
- [6] N. Nishi, T. Uruga, H. Tanida, T. Kakiuchi, Temperature Dependence of Multilayering at the Free Surface of Ionic Liquids Probed by X-ray Reflectivity Measurements, *Langmuir*. 27 (2011) 7531–7536. <https://doi.org/10.1021/la200252z>.
- [7] P. Reichert, K.S. Kjær, T.B. van Driel, J. Mars, J.W. Ochsmann, D. Pontoni, M. Deutsch, M.M. Nielsen, M. Mezger, Molecular scale structure and dynamics at an ionic liquid/electrode interface, *Faraday Discuss.* 206 (2017) 141–157. <https://doi.org/10.1039/C7FD00171A>.
- [8] M. Mezger, R. Roth, H. Schröder, P. Reichert, D. Pontoni, H. Reichert, Solid-liquid interfaces of ionic liquid solutions—Interfacial layering and bulk correlations, *J. Chem. Phys.* 142 (2015) 164707. <https://doi.org/10.1063/1.4918742>.
- [9] T.A. Petach, A. Mehta, R. Marks, B. Johnson, M.F. Toney, D. Goldhaber-Gordon, Voltage-Controlled Interfacial Layering in an Ionic Liquid on SrTiO₃, *ACS Nano*. 10 (2016) 4565–4569. <https://doi.org/10.1021/acsnano.6b00645>.
- [10] M. Chu, M. Miller, P. Dutta, Crowding and Anomalous Capacitance at an Electrode–Ionic Liquid Interface Observed Using Operando X-ray Scattering, *ACS Cent. Sci.* 2 (2016) 175–180. <https://doi.org/10.1021/acscentsci.6b00014>.

- [11] N. Nishi, J. Uchiyashiki, Y. Ikeda, S. Katakura, T. Oda, M. Hino, N.L. Yamada, Potential-Dependent Structure of the Ionic Layer at the Electrode Interface of an Ionic Liquid Probed Using Neutron Reflectometry, *J. Phys. Chem. C.* 123 (2019) 9223–9230. <https://doi.org/10.1021/acs.jpcc.9b01151>.
- [12] S. Katakura, K. Amano, T. Sakka, W. Bu, B. Lin, M.L. Schlossman, N. Nishi, Evolution and Reversible Polarity of Multilayering at the Ionic Liquid/Water Interface, *J. Phys. Chem. B.* 124 (2020) 6412–6419. <https://doi.org/10.1021/acs.jpcb.0c03711>.
- [13] S. Katakura, N. Nishi, K. Kobayashi, K. Amano, T. Sakka, Effect of Switching the Length of Alkyl Chains on Electric Double Layer Structure and Differential Capacitance at the Electrode Interface of Quaternary Ammonium-Based Ionic Liquids Studied Using Molecular Dynamics Simulation, *J. Phys. Chem. C.* 124 (2020) 7873–7883. <https://doi.org/10.1021/acs.jpcc.0c00795>.
- [14] S. Zhang, T. Sakka, N. Nishi, Slow and Fast Dynamics at the Ionic Liquid/Gold Electrode Interface Separately Probed by Electrochemical Surface Plasmon Resonance Combined with Sequential Potential Pulse Techniques, *J. Electrochem. Soc.* (2022). <https://doi.org/10.1149/1945-7111/ac58c4>.
- [15] A. Uysal, H. Zhou, G. Feng, S.S. Lee, S. Li, P.T. Cummings, P.F. Fulvio, S. Dai, J.K. McDonough, Y. Gogotsi, P. Fenter, Interfacial ionic ‘liquids’: connecting static and dynamic structures, *J. Phys. Condens. Matter.* 27 (2015) 032101. <https://doi.org/10.1088/0953-8984/27/3/032101>.
- [16] Y.-Z. Su, J.-W. Yan, M.-G. Li, Z.-X. Xie, B.-W. Mao, Z.-Q. Tian, Adsorption of Solvent Cations on Au(111) and Au(100) in Alkylimidazolium-Based Ionic Liquids - Worm-Like versus Micelle-Like Structures, *Z. Phys. Chem.-Int. J. Res.* 226 (2012) 979–994. <https://doi.org/10.1524/zpch.2012.0255>.
- [17] A.J. Page, A. Elbourne, R. Stefanovic, M.A. Addicoat, G.G. Warr, K. Voïtchovsky, R. Atkin, 3-Dimensional atomic scale structure of the ionic liquid-graphite interface elucidated by AM-AFM and quantum chemical simulations, *Nanoscale.* 6 (2014) 8100–8106. <https://doi.org/10.1039/C4NR01219D>.
- [18] N. Borisenko, S.Z. El Abedin, F. Endres, An in Situ STM and DTS Study of the Extremely Pure [EMIM]FAP/Au(111) Interface, *Chemphyschem.* 13 (2012) 1736–1742. <https://doi.org/10.1002/cphc.201100873>.
- [19] F. Buchner, K. Forster-Tonigold, B. Uhl, D. Alwast, N. Wagner, A. Groß, R.J. Behm, Towards the Microscopic Identification of Anions and Cations at the Ionic Liquid | Ag(111) Interface: A Combined Experimental and Theoretical Investigation, *ACS Nano.* 7 (2013) 7773–7784.
- [20] J. Hoth, F. Hausen, M.H. Müser, R. Bennewitz, Force microscopy of layering and friction in an ionic liquid, *J. Phys. Condens. Matter.* 26 (2014) 284110. <https://doi.org/10.1088/0953-8984/26/28/284110>.
- [21] J.M. Black, D. Walters, A. Labuda, G. Feng, P.C. Hillesheim, S. Dai, P.T. Cummings, S.V. Kalinin, R. Proksch, N. Balke, Bias-Dependent Molecular-Level Structure of Electrical Double Layer in Ionic Liquid on Graphite, *Nano Lett.* 13 (2013) 5954–5960. <https://doi.org/10.1021/nl4031083>.
- [22] R. Atkin, N. Borisenko, M. Drüscher, S.Z. El Abedin, F. Endres, R. Hayes, B. Huber, B. Roling, An in situ STM/AFM and impedance spectroscopy study of the extremely pure 1-butyl-1-methylpyrrolidinium

- tris(pentafluoroethyl)trifluorophosphate/Au(111) interface: potential dependent solvation layers and the herringbone reconstruction, *Phys. Chem. Chem. Phys.* 13 (2011) 6849–6857. <https://doi.org/10.1039/c0cp02846k>.
- [23] X. Gong, A. Kozbial, F. Rose, L. Li, Effect of π - π + Stacking on the Layering of Ionic Liquids Confined to an Amorphous Carbon Surface, *ACS Appl. Mater. Interfaces*. 7 (2015) 7078–7081. <https://doi.org/10.1021/acsami.5b01140>.
- [24] X. Gong, A. Kozbial, L. Li, What causes extended layering of ionic liquids on the mica surface?, *Chem. Sci.* 6 (2015) 3478–3482. <https://doi.org/10.1039/C5SC00832H>.
- [25] A. Elbourne, S. McDonald, K. Voïchovsky, F. Endres, G.G. Warr, R. Atkin, Nanostructure of the Ionic Liquid–Graphite Stern Layer, *ACS Nano*. 9 (2015) 7608–7620. <https://doi.org/10.1021/acsnano.5b02921>.
- [26] L.A. Jurado, R.M. Espinosa-Marzal, Insight into the Electrical Double Layer of an Ionic Liquid on Graphene, *Sci. Rep.* 7 (2017) 4225. <https://doi.org/10.1038/s41598-017-04576-x>.
- [27] M.-G. Li, L. Chen, Y.-X. Zhong, Z.-B. Chen, J.-W. Yan, B.-W. Mao, The electrochemical interface of Ag(111) in 1-ethyl-3-methylimidazolium bis(trifluoromethylsulfonyl)imide ionic liquid—A combined in-situ scanning probe microscopy and impedance study, *Electrochimica Acta*. 197 (2016) 282–289. <https://doi.org/10.1016/j.electacta.2015.12.227>.
- [28] N. Hjalmarsson, R. Atkin, M.W. Rutland, Is the boundary layer of an ionic liquid equally lubricating at higher temperature?, *Phys. Chem. Chem. Phys.* 18 (2016) 9232–9239. <https://doi.org/10.1039/C5CP05837F>.
- [29] V. Lockett, M. Horne, R. Sedev, T. Rodopoulos, J. Ralston, Differential capacitance of the double layer at the electrode/ionic liquids interface, *Phys. Chem. Chem. Phys.* 12 (2010) 12499–12512. <https://doi.org/10.1039/c0cp00170h>.
- [30] M. Gnahn, C. Berger, M. Arkhipova, H. Kunkel, T. Pajkossy, G. Maas, D.M. Kolb, The interfaces of Au(111) and Au(100) in a hexaalkyl-substituted guanidinium ionic liquid: an electrochemical and in situ STM study, *Phys. Chem. Chem. Phys.* 14 (2012) 10647–10652. <https://doi.org/10.1039/C2CP41084B>.
- [31] M. Gnahn, C. Müller, R. Répánszki, T. Pajkossy, D.M. Kolb, The interface between Au(100) and 1-butyl-3-methyl-imidazolium-hexafluorophosphate, *Phys. Chem. Chem. Phys.* 13 (2011) 11627–11633. <https://doi.org/10.1039/c1cp20562e>.
- [32] J. Wallauer, M. Drüscher, B. Huber, B. Roling, The Differential Capacitance of Ionic Liquid | Metal Electrode Interfaces – A Critical Comparison of Experimental Results with Theoretical Predictions, *Z. Für Naturforschung B*. 68b (2013) 1143–1153. <https://doi.org/10.5560/ZNB.2013-3153>.
- [33] Y. Su, J. Yan, M. Li, M. Zhang, B. Mao, Electric Double Layer of Au(100)/Imidazolium-Based Ionic Liquids Interface: Effect of Cation Size, *J. Phys. Chem. C*. 117 (2013) 205–212. <https://doi.org/10.1021/jp3079919>.
- [34] C. Gomes, R. Costa, C.M. Pereira, A.F. Silva, The electrical double layer at the ionic liquid/Au and Pt electrode interface, *RSC Adv.* 4 (2014) 28914–28921. <https://doi.org/10.1039/C4RA03977G>.
- [35] R. Costa, I.V. Voroshlova, M.N.D.S. Cordeiro, C.M. Pereira, A.F. Silva, Enhancement of differential double layer capacitance and charge accumulation by tuning the composition of ionic liquids mixtures, *Electrochimica Acta*. 261 (2018)

- 214–220. <https://doi.org/10.1016/j.electacta.2017.12.134>.
- [36] N. Zhang, X.-R. Wang, Y.-X. Yuan, H.-F. Wang, M.-M. Xu, Z.-G. Ren, J.-L. Yao, R.-A. Gu, Probing double layer structure at Au/[BMIm]BF₄ interface by molecular length-dependent SERS Stark effect, *J. Electroanal. Chem.* 751 (2015) 137–143. <https://doi.org/10.1016/j.jelechem.2015.05.041>.
- [37] G.-B. Pan, W. Freyland, 2D phase transition of PF₆ adlayers at the electrified ionic liquid/Au(111) interface, *Chem. Phys. Lett.* 427 (2006) 96–100. <https://doi.org/10.1016/j.cplett.2006.05.114>.
- [38] Y.-Z. Su, Y.-C. Fu, J.-W. Yan, Z.-B. Chen, B.-W. Mao, Double Layer of Au(100)/Ionic Liquid Interface and Its Stability in Imidazolium-Based Ionic Liquids, *Angew. Chem. Int. Ed.* 48 (2009) 5148–5151. <https://doi.org/10.1002/anie.200900300>.
- [39] T. Pajkossy, C. Müller, T. Jacob, The metal–ionic liquid interface as characterized by impedance spectroscopy and in situ scanning tunneling microscopy, *Phys. Chem. Chem. Phys.* 20 (2018) 21241–21250. <https://doi.org/10.1039/C8CP02074D>.
- [40] J.M. Klein, H. Squire, B. Gurkan, Electroanalytical Investigation of the Electrode–Electrolyte Interface of Quaternary Ammonium Ionic Liquids: Impact of Alkyl Chain Length and Ether Functionality, *J. Phys. Chem. C.* 124 (2020) 5613–5623. <https://doi.org/10.1021/acs.jpcc.9b08016>.
- [41] W. Dean, J. Klein, B. Gurkan, Do Deep Eutectic Solvents Behave Like Ionic Liquid Electrolytes? A Perspective from the Electrode-Electrolyte Interface, *J. Electrochem. Soc.* 168 (2021) 026503. <https://doi.org/10.1149/1945-7111/abde83>.
- [42] M. Belotti, X. Lyu, L. Xu, P. Halat, N. Darwish, D.S. Silvester, C. Goh, E.I. Izgorodina, M.L. Coote, S. Ciampi, Experimental Evidence of Long-Lived Electric Fields of Ionic Liquid Bilayers, *J. Am. Chem. Soc.* 143 (2021) 17431–17440. <https://doi.org/10.1021/jacs.1c06385>.
- [43] N. Hjalmarsson, D. Wallinder, S. Glavatskikh, R. Atkin, T. Aastrup, M.W. Rutland, Weighing the surface charge of an ionic liquid, *Nanoscale.* 7 (2015) 16039–16045. <https://doi.org/10.1039/C5NR03965G>.
- [44] M. Schammer, A. Latz, B. Horstmann, The Role of Energy Scales for the Structure of Ionic Liquids at Electrified Interfaces: A Theory-Based Approach, *J. Phys. Chem. B.* 126 (2022) 2761–2776. <https://doi.org/10.1021/acs.jpcb.2c00215>.
- [45] M.Z. Bazant, B.D. Storey, A.A. Kornyshev, Double Layer in Ionic Liquids: Overscreening versus Crowding, *Phys. Rev. Lett.* 106 (2011) 046102. <https://doi.org/10.1103/PhysRevLett.106.046102>.
- [46] J.P. de Souza, Z.A.H. Goodwin, M. McEldrew, A.A. Kornyshev, M.Z. Bazant, Interfacial Layering in the Electric Double Layer of Ionic Liquids, *Phys. Rev. Lett.* 125 (2020) 116001. <https://doi.org/10.1103/PhysRevLett.125.116001>.
- [47] N. Gavish, A. Yochelis, Theory of Phase Separation and Polarization for Pure Ionic Liquids, *J. Phys. Chem. Lett.* 7 (2016) 1121–1126. <https://doi.org/10.1021/acs.jpclett.6b00370>.
- [48] M.V. Fedorov, A.A. Kornyshev, Towards understanding the structure and capacitance of electrical double layer in ionic liquids, *Electrochimica Acta.* 53 (2008) 6835–6840. <https://doi.org/10.1016/j.electacta.2008.02.065>.
- [49] M.V. Fedorov, A.A. Kornyshev, Ionic Liquid Near a Charged Wall: Structure and Capacitance of Electrical Double Layer, *J. Phys. Chem. B.* 112 (2008) 11868–11872. <https://doi.org/10.1021/jp803440q>.

- [50] M. Girotto, A.M. Alencar, Modified 3D Ewald Summation for Slab Geometry at Constant Potential, *J. Phys. Chem. B.* 124 (2020) 7842–7848.
<https://doi.org/10.1021/acs.jpcb.0c03510>.
- [51] J.L. Ma, Q. Meng, J. Fan, Charge driven lateral structural evolution of ions in electric double layer capacitors strongly correlates with differential capacitance, *Phys. Chem. Chem. Phys.* 20 (2018) 8054–8063.
<https://doi.org/10.1039/C7CP08075A>.
- [52] S. Begić, F. Chen, E. Jónsson, M. Forsyth, Overscreening and crowding in electrochemical ionic liquid systems, *Phys. Rev. Mater.* 3 (2019) 095801.
<https://doi.org/10.1103/PhysRevMaterials.3.095801>.
- [53] K. Kirchner, T. Kirchner, V. Ivaništšev, M.V. Fedorov, Electrical double layer in ionic liquids: Structural transitions from multilayer to monolayer structure at the interface, *Electrochimica Acta*. 110 (2013) 762–771.
<https://doi.org/10.1016/j.electacta.2013.05.049>.
- [54] V. Ivaništšev, S. O'Connor, M.V. Fedorov, Poly(a)morphic portrait of the electrical double layer in ionic liquids, *Electrochim. Commun.* 48 (2014) 61–64.
<https://doi.org/10.1016/j.elecom.2014.08.014>.
- [55] I.V. Voroshylova, H. Ers, V. Koverga, B. Docampo-Álvarez, P. Pikma, V.B. Ivaništšev, M.N.D.S. Cordeiro, Ionic liquid–metal interface: The origins of capacitance peaks, *Electrochimica Acta*. 379 (2021) 138148.
<https://doi.org/10.1016/j.electacta.2021.138148>.
- [56] N. Georgi, A.A. Kornyshev, M.V. Fedorov, The anatomy of the double layer and capacitance in ionic liquids with anisotropic ions: Electrostriction vs. lattice saturation, *J. Electroanal. Chem.* 649 (2010) 261–267.
- [57] S. Sharma, H.K. Kashyap, Structure of Quaternary Ammonium Ionic Liquids at Interfaces: Effects of Cation Tail Modification with Isoelectronic Groups, *J. Phys. Chem. C*. 119 (2015) 23955–23967. <https://doi.org/10.1021/acs.jpcc.5b06460>.
- [58] S.A. Kislenko, Yu.O. Moroz, K. Karu, V.B. Ivaništšev, M.V. Fedorov, Calculating the Maximum Density of the Surface Packing of Ions in Ionic Liquids, *Russ. J. Phys. Chem. A*. 92 (2018) 999–1005. <https://doi.org/10.1134/S0036024418050187>.
- [59] R.M. Lynden-Bell, M.G. Del Pópolo, T.G.A. Youngs, J. Kohanoff, C.G. Hanke, J.B. Harper, C.C. Pinilla, Simulations of Ionic Liquids, Solutions, and Surfaces, *Acc. Chem. Res.* 40 (2007) 1138–1145. <https://doi.org/10.1021/ar700065s>.
- [60] C. Merlet, B. Rotenberg, P.A. Madden, M. Salanne, Computer simulations of ionic liquids at electrochemical interfaces, *Phys. Chem. Chem. Phys.* 15 (2013) 15781–15792.
- [61] J. Vatamanu, D. Bedrov, O. Borodin, On the application of constant electrode potential simulation techniques in atomistic modelling of electric double layers, *Mol. Simul.* 43 (2017) 838–849. <https://doi.org/10.1080/08927022.2017.1279287>.
- [62] L. Scalfi, M. Salanne, B. Rotenberg, Molecular Simulation of Electrode-Solution Interfaces, *Annu. Rev. Phys. Chem.* 72 (2021) 189–212.
<https://doi.org/10.1146/annurev-physchem-090519-024042>.
- [63] T. Dufils, G. Jeanmairet, B. Rotenberg, M. Sprik, M. Salanne, Simulating Electrochemical Systems by Combining the Finite Field Method with a Constant Potential Electrode, *Phys. Rev. Lett.* 123 (2019).
<https://doi.org/10.1103/PhysRevLett.123.195501>.

- [64] A. Groß, Structure of Electrode-Electrolyte Interfaces, Modeling of Double Layer and Electrode Potential, in: W. Andreoni, S. Yip (Eds.), *Handb. Mater. Model.*, Springer International Publishing, Cham, 2020: pp. 1439–1472.
https://doi.org/10.1007/978-3-319-44680-6_7.
- [65] A.H. Larsen, J.J. Mortensen, J. Blomqvist, I.E. Castelli, R. Christensen, M. Dulak, J. Friis, M.N. Groves, B. Hammer, C. Hargus, E.D. Hermes, P.C. Jennings, P.B. Jensen, J. Kermode, J.R. Kitchin, E.L. Kolsbjergr, J. Kubal, K. Kaasbjergr, S. Lysgaard, J.B. Maronsson, T. Maxson, T. Olsen, L. Pastewka, A. Peterson, C. Rostgaard, J. Schiøtz, O. Schütt, M. Strange, K.S. Thygesen, T. Vegge, L. Vilhelmsen, M. Walter, Z. Zeng, K.W. Jacobsen, The atomic simulation environment—a Python library for working with atoms, *J. Phys. Condens. Matter.* 29 (2017) 273002.
<https://doi.org/10.1088/1361-648X/aa680e>.
- [66] L. Martínez, R. Andrade, E.G. Birgin, J.M. Martínez, PACKMOL: A Package for Building Initial Configurations for Molecular Dynamics Simulations, *J. Comput. Chem.* 30 (2009) 2157–2164. <https://doi.org/10.1002/jcc.21224>.
- [67] C. Schröder, Comparing reduced partial charge models with polarizable simulations of ionic liquids, *Phys. Chem. Chem. Phys.* 14 (2012) 3089–3102.
<https://doi.org/10.1039/C2CP23329K>.
- [68] I.V. Voroshyllova, M. Lembinen, H. Ers, M. Mišin, V.A. Koverga, C.M. Pereira, V.B. Ivaništšev, M.N.D.S. Cordeiro, On the role of the surface charge plane position at Au(hkl)–BMImPF₆ interfaces, *Electrochimica Acta.* 318 (2019) 76–82.
<https://doi.org/10.1016/j.electacta.2019.05.058>.
- [69] N.D. Lang, W. Kohn, Theory of Metal Surfaces: Induced Surface Charge and Image Potential, *Phys. Rev. B.* 7 (1973) 3541–3550.
<https://doi.org/10.1103/physrevb.7.3541>.
- [70] N.D. Lang, W. Kohn, Theory of Metal Surfaces: Work Function, *Phys. Rev. B.* 3 (1971) 1215–1223. <https://doi.org/10.1103/PhysRevB.3.1215>.
- [71] N.B. Luque, W. Schmickler, The electric double layer on graphite, *Electrochimica Acta.* 71 (2012) 82–85. <https://doi.org/10.1016/j.electacta.2012.03.083>.
- [72] A.A. Kornyshev, N.B. Luque, W. Schmickler, Differential capacitance of ionic liquid interface with graphite: the story of two double layers, *J. Solid State Electrochem.* 18 (2014) 1345–1349.
- [73] E. Roos Nerut, K. Karu, I.V. Voroshyllova, K. Kirchner, T. Kirchner, M.V. Fedorov, V.B. Ivaništšev, NaRIBaS—A Scripting Framework for Computational Modeling of Nanomaterials and Room Temperature Ionic Liquids in Bulk and Slab, *Computation.* 6 (2018) 57. <https://doi.org/10.3390/computation6040057>.
- [74] O.M. Magnussen, Ordered Anion Adlayers on Metal Electrode Surfaces, *Chem. Rev.* 102 (2002) 679–726. <https://doi.org/10.1021/cr000069p>.
- [75] C. Noh, Y. Jung, Understanding the charging dynamics of an ionic liquid electric double layer capacitor via molecular dynamics simulations, *Phys. Chem. Chem. Phys.* 21 (2019) 6790–6800. <https://doi.org/10.1039/C8CP07200K>.
- [76] F. Tang, T. Ohto, T. Hasegawa, M. Bonn, Y. Nagata, $\pi+-\pi+$ stacking of imidazolium cations enhances molecular layering of room temperature ionic liquids at their interfaces, *Phys Chem Chem Phys.* 19 (2017) 2850–2856.
<https://doi.org/10.1039/C6CP07034E>.
- [77] A.J.L. Costa, M.R.C. Soromenho, K. Shimizu, I.M. Marrucho, J.M.S.S. Esperança,

- J.N.C. Lopes, L.P.N. Rebelo, Density, Thermal Expansion and Viscosity of Cholinium-Derived Ionic Liquids, *ChemPhysChem.* 13 (2012) 1902–1909. <https://doi.org/10.1002/cphc.201100852>.
- [78] M. Součková, J. Klomfar, J. Pátek, Surface tension and 0.1 MPa densities of imidazolium-, pyridinium-, pyrrolidinium-, and piperidinium-based tris(pentafluoroethyl)trifluorophosphate ionic liquids, *Fluid Phase Equilibria.* 333 (2012) 38–46. <https://doi.org/10.1016/j.fluid.2012.07.013>.
- [79] W. Humphrey, A. Dalke, K. Schulten, VMD: Visual molecular dynamics, *J. Mol. Graph.* 14 (1996) 33–38. [https://doi.org/10.1016/0263-7855\(96\)00018-5](https://doi.org/10.1016/0263-7855(96)00018-5).
- [80] S. Grimme, A. Hansen, S. Ehlert, J.-M. Mewes, r2SCAN-3c: A “Swiss army knife” composite electronic-structure method, *J. Chem. Phys.* 154 (2021) 064103. <https://doi.org/10.1063/5.0040021>.
- [81] F. Neese, F. Wennmohs, U. Becker, C. Riplinger, The ORCA quantum chemistry program package, *J. Chem. Phys.* 152 (2020) 224108. <https://doi.org/10.1063/5.0004608>.
- [82] O. Oll, C. Siimenson, K. Lust, G. Gorbatovski, E. Lust, Specific adsorption from an ionic liquid: impedance study of iodide ion adsorption from a pure halide ionic liquid at bismuth single crystal planes, *Electrochimica Acta.* 247 (2017) 910–919. <https://doi.org/10.1016/j.electacta.2017.07.034>.
- [83] X. Zhang, Y.-X. Zhong, J.-W. Yan, Y.-Z. Su, M. Zhang, B.-W. Mao, Probing double layer structures of Au (111)–BMIPF 6 ionic liquid interfaces from potential-dependent AFM force curves, *Chem. Commun.* 48 (2012) 582–584. <https://doi.org/10.1039/C1CC15463J>.
- [84] E. Anderson, V. Grozovski, L. Siinor, C. Siimenson, E. Lust, In situ STM studies of Bi(111)|1-ethyl-3-methylimidazolium tetrafluoroborate + 1-ethyl-3-methylimidazolium iodide interface, *Electrochem. Commun.* 46 (2014) 18–21. <https://doi.org/10.1016/j.elecom.2014.05.032>.
- [85] R. Wen, B. Rahn, O.M. Magnussen, Potential-Dependent Adlayer Structure and Dynamics at the Ionic Liquid/Au(111) Interface: A Molecular-Scale In Situ Video-STM Study, *Angew. Chem. Int. Ed.* 54 (2015) 6062–6066. <https://doi.org/10.1002/anie.201501715>.
- [86] H. Kruse, S. Grimme, A geometrical correction for the inter- and intra-molecular basis set superposition error in Hartree-Fock and density functional theory calculations for large systems, *J. Chem. Phys.* 136 (2012) 154101. <https://doi.org/10.1063/1.3700154>.
- [87] Y. Fu, A.V. Rudnev, Scanning probe microscopy of an electrode/ionic liquid interface, *Curr. Opin. Electrochem.* 1 (2017) 59–65. <https://doi.org/10.1016/j.coelec.2017.01.005>.
- [88] I.V. Voroshylova, H. Ers, B. Docampo-Álvarez, P. Pikma, V.B. Ivaniščev, M.N.D.S. Cordeiro, Hysteresis in the MD Simulations of Differential Capacitance at the Ionic Liquid–Au Interface, *J. Phys. Chem. Lett.* 11 (2020) 10408–10413. <https://doi.org/10.1021/acs.jpclett.0c03212>.
- [89] S. Baldelli, Surface Structure at the Ionic Liquid–Electrified Metal Interface, *Acc. Chem. Res.* 41 (2008) 421–431. <https://doi.org/10.1021/ar700185h>.
- [90] Z. Dai, Y. You, Y. Zhu, S. Wang, W. Zhu, X. Lu, Atomistic Insights into the Layered Microstructure and Time-Dependent Stability of [BMIM][PF₆] Confined within

- the Meso-Slit of Carbon, *J. Phys. Chem. B.* 123 (2019) 6857–6869.
<https://doi.org/10.1021/acs.jpcb.9b02682>.
- [91] E.S.C. Ferreira, C.M. Pereira, M.N.D.S. Cordeiro, D.J.V.A. dos Santos, Molecular Dynamics Study of the Gold/Ionic Liquids Interface, *J. Phys. Chem. B.* 119 (2015) 9883–9892. <https://doi.org/10.1021/acs.jpcb.5b04505>.
- [92] A.M. Smith, K.R.J. Lovelock, N.N. Gosvami, P. Licence, A. Dolan, T. Welton, S. Perkin, Monolayer to Bilayer Structural Transition in Confined Pyrrolidinium-Based Ionic Liquids, *J. Phys. Chem. Lett.* 4 (2013) 378–382. <https://doi.org/10.1021/jz301965d>.
- [93] S. Perkin, L. Crowhurst, H. Niedermeyer, T. Welton, A.M. Smith, N.N. Gosvami, Self-assembly in the electrical double layer of ionic liquids, *Chem. Commun.* 47 (2011) 6572–6574. <https://doi.org/10.1039/C1CC11322D>.
- [94] S. Watanabe, G.A. Pilkington, A. Oleshkevych, P. Pedraz, M. Radiom, R. Welbourn, S. Glavatskikh, M.W. Rutland, Interfacial structuring of non-halogenated imidazolium ionic liquids at charged surfaces: effect of alkyl chain length, *Phys. Chem. Chem. Phys.* 22 (2020) 8450–8460. <https://doi.org/10.1039/D0CP00360C>.
- [95] V. Ivaniščev, M.V. Fedorov, Interfaces between Charged Surfaces and Ionic Liquids: Insights from Molecular Simulations, *Electrochim. Soc. Interface.* 23 (2014) 65–69. <https://doi.org/10.1149/2.F08141if>.
- [96] W.M. Haynes, D.R. Lide, T.J. Bruno, CRC handbook of chemistry and physics, CRC press Boca Raton, FL, 2017.
- [97] E. Anderson, V. Grozovski, L. Siinor, C. Siimenson, V. Ivaniščev, K. Lust, S. Kallip, E. Lust, Influence of the electrode potential and in situ STM scanning conditions on the phase boundary structure of the single crystal Bi(1 1 1)|1-butyl-4-methylpyridinium tetrafluoroborate interface, *J. Electroanal. Chem.* 709 (2013) 46–56. <https://doi.org/10.1016/j.jelechem.2013.10.004>.
- [98] O. Oll, M. Väärtnöu, G. Gorbatovski, J. Zhao, C. Siimenson, L. Siinor, K. Lust, T. Romann, P. Pikma, E. Lust, Adsorption of anions on bismuth and cadmium single crystal plane electrodes from various solvents and ionic liquid mixtures, *Electrochimica Acta.* 319 (2019) 895–908. <https://doi.org/10.1016/j.electacta.2019.06.179>.
- [99] S. Snegir, Y.J. Dappe, D. Sysoiev, O. Pluchery, T. Huhn, E. Scheer, Where do the counterions go? Tip-induced dissociation of self-assembled triazatriangulenium-based molecules on Au(111), *Phys. Chem. Chem. Phys.* 23 (2021) 9930–9937. <https://doi.org/10.1039/D1CP00221J>.
- [100] R. Wen, B. Rahn, Olaf.M. Magnussen, In Situ Video-STM Study of Adlayer Structure and Surface Dynamics at the Ionic Liquid/Au (111) Interface, *J. Phys. Chem. C.* 120 (2016) 15765–15771. <https://doi.org/10.1021/acs.jpcc.5b11590>.
- [101] W.-Y. Tsai, J. Come, W. Zhao, R. Wang, G. Feng, B. Prasad Thapaliya, S. Dai, L. Collins, N. Balke, Hysteretic order-disorder transitions of ionic liquid double layer structure on graphite, *Nano Energy.* 60 (2019) 886–893. <https://doi.org/10.1016/j.nanoen.2019.04.022>.
- [102] I. Borukhov, D. Andelman, H. Orland, Adsorption of large ions from an electrolyte solution: a modified Poisson–Boltzmann equation, *Electrochimica Acta.* 46 (2000) 221–229. [https://doi.org/10.1016/S0013-4686\(00\)00576-4](https://doi.org/10.1016/S0013-4686(00)00576-4).
- [103] I. Borukhov, D. Andelman, H. Orland, Steric Effects in Electrolytes: A Modified

- Poisson-Boltzmann Equation, Phys. Rev. Lett. 79 (1997) 435–438.
<https://doi.org/10.1103/PhysRevLett.79.435>.
- [104] D.M. Hudgins, Jr. Charles W. Bauschlicher, L.J. Allamandola, Variations in the Peak Position of the 6.2 μ m Interstellar Emission Feature: A Tracer of N in the Interstellar Polycyclic Aromatic Hydrocarbon Population, Astrophys. J. 632 (2005) 316–332. <https://doi.org/10.1086/432495>.
- [105] L.-F. Velázquez-López, S.-M. Pacheco-Ortín, R. Mejía-Olvera, E. Agacino-Valdés, DFT study of CO adsorption on nitrogen/boron doped-graphene for sensor applications, J. Mol. Model. 25 (2019) 91.
<https://doi.org/10.1007/s00894-019-3973-z>.
- [106] S. Lemke, S. Ulrich, F. Claußen, A. Bloedorn, U. Jung, R. Herges, O.M. Magnussen, Triazatriangulenium adlayers on Au(111): Superstructure as a function of alkyl side chain length, Surf. Sci. 632 (2015) 71–76. <https://doi.org/10.1016/j.susc.2014.08.028>.
- [107] S. Ulrich, U. Jung, T. Strunskus, C. Schütt, A. Bloedorn, S. Lemke, E. Ludwig, L. Kipp, F. Faupel, O. Magnussen, R. Herges, X-ray spectroscopy characterization of azobenzene-functionalized triazatriangulenium adlayers on Au(111) surfaces, Phys. Chem. Chem. Phys. 17 (2015) 17053–17062.
<https://doi.org/10.1039/C5CP01447F>.
- [108] M.Z. Bazant, M.S. Kilic, B.D. Storey, A. Ajdari, Towards an understanding of induced-charge electrokinetics at large applied voltages in concentrated solutions, Adv. Colloid Interface Sci. 152 (2009) 48–88.
<https://doi.org/10.1016/j.cis.2009.10.001>.